Discovery of a new craniofacial gene influencing adaptive phenotypes in a non-model pupfish radiation

M. Fernanda Palominos[1,2], Vanessa Muhl[1,2], Emilie J. Richards[3], Christopher H. Martin[1,2]

[1]Department of Integrative Biology, University of California, Berkeley

[2]Museum of Vertebrate Zoology, University of California, Berkeley

[3]Department of Ecology, Evolution, and Behavior, University of Minnesota

Keywords: gene expression, fluorescence in situ hybridization, galanin, trophic morphology, craniofacial divergence, evo devo, speciation, adaptive radiation

Abstract

Understanding the origins of new species with novel adaptations is a fundamental question in biology that also provides an opportunity to uncover new genes and regulatory networks with potential clinical relevance. Here we demonstrate a new role for *galr2* in vertebrate craniofacial development using a non-model adaptive radiation of trophic specialist pupfishes endemic to San Salvador Island in the Bahamas. We confirmed the loss of a *Sry* transcription factor binding site in scale-eating pupfish and found significant spatial differences in *galr2* expression among pupfish species in the Meckel's cartilage and premaxilla using in situ hybridization. We then experimentally confirmed a novel function for Galr2 in craniofacial development and jaw elongation by exposing embryos to Galr2. Galr2-inhibition reduced Meckel's cartilage length and increased chondrocyte density in both trophic specialists but not in the generalist genetic background. We propose a mechanism for jaw elongation in scale-eaters based on the reduced expression of *galr2* putatively due to the loss of the *Sry* binding site that results in reduced opportunities for binding with their endogenous ligand during craniofacial chondrogenesis. Fewer Galr2 receptors in the scale-eater Meckel's cartilage may result in their enlarged jaw lengths as adults by limiting opportunities for Galr2 antagonists to bind to these receptors during development. Our findings illustrate the growing utility of linking candidate adaptive SNPs in non-model vertebrate systems with highly divergent phenotypes to novel gene functions with potential implications for human biology.

Introduction

Craniofacial developmental anomalies are the most common source of birth defects in humans, present in 1 out of 700 births (Hall et al., 2010; Meng et al., 2009; Palmer et al., 2016). While Mendelian craniofacial defects are well characterized (e.g. Treacher Collins Syndrome (Kadakia et al., 2014), Apert Syndrome (Wilkie et al., 1995), and Crouzon Syndrome (Helman et al., 2014; Reardon et al., 1994)), the developmental genetics of complex craniofacial defects, such as non-syndromic orofacial clefts and craniosynostosis, are poorly understood (Carlborg and Haley, 2004; Glazier, 2002; Hirschhorn and Daly, 2005; Hochheiser et al., 2011; Manolio et al., 2009; Monteiro and Podlaha, 2009; Weinberg et al., 2018). With the continued lowering costs of genomic sequencing and functional genetic tools, it is increasingly feasible to develop new genetic models for understanding human development and disease.

Current knowledge of craniofacial developmental genetics results mainly from mutagenic screens and forward genetic approaches in a few vertebrate model systems (primarily mice and zebrafish); however, these approaches are typically biased toward large Mendelian effects on easily detectable phenotypes, often missing the variation most relevant to common craniofacial birth defects in humans, such as small-effect variants, subtle differences in skeletal shape, and epistatic interactions among genes and the environment (Albertson et al., 2009; Powder and Albertson, 2016; Roberts et al., 2011). Conversely, complementary genome-wide association studies (GWAS) of craniofacial syndromes and normal-range facial variation in humans often reveal small-effect loci with no tractable possibilities for functional interrogation (Bonfante et al., 2021; Naqvi et al., 2022; Weinberg et al., 2018). Thus, understanding the genetic bases of naturally occurring, highly divergent adaptive phenotypes in non-model systems that parallel human clinical variation, known as ‘evolutionary mutant’ models (Albertson et al., 2009; Concannon and

Albertson, 2015; Powder and Albertson, 2016; Rohner, 2018), provides a powerful approach combining the tractable functional investigations possible in model systems with genome-wide association scans of small-effect regulatory loci underlying natural craniofacial diversity. For example, novel insights into a broad diversity of human diseases have now arisen from studies of diverse non-model species experiencing strong selective pressures in nature, including senescence (i.e., naked mole rat (Buffenstein, 2008); turquoise killifish (Platzer and Englert, 2016), and rockfish (Kolora et al., 2021)); eye degeneration, bone loss and enhanced lipogenesis (blind cavefishes (Gross et al., 2016; Hofmann et al., 2009; Protas et al., 2007; Lam et al. 2022)); body size (domesticated dogs (Sutter et al., 2007)); cholesterol (polar bears (Liu et al., 2014)); and diabetes (dolphins (Venn-watson et al., 2011)). In particular, the most remarkable diversity of vertebrate craniofacial morphology is represented in teleost fishes, often associated with their diverse and sometimes highly specialized modes of feeding (e.g., Liem, 1991; Otten, 1983; Albertson et al., 2003; Martin and Richards 2019; Konings et al., 2021; Evans et al. 2021).

Emerging fish model systems include the rapidly evolving East African and Cameroon cichlid radiations, in which a small number of genetic changes underlie immense morphological disparity in over 1,500 cichlid species (Brawand et al., 2014; Conith et al., 2019; Kocher et al., 2003; Martin, 2012; Martin, 2013; Martin and Genner, 2009; Navon et al., 2020) and the repeated parallel speciation of stickleback ecomorphs in glacial lakes (Chan et al., 2010; Erickson et al., 2016; Jones et al., 2012; Miller et al., 2007; Ishikawa et al. 2019). These systems provide excellent examples of leveraging naturally-occurring and highly divergent craniofacial phenotypes as 'evolutionary mutants' or 'evolutionary forward genetics' models to gain novel insights into the genetics of natural human craniofacial variation (Erickson et al., 2014; Glazer et al., 2015; J. Parsons et al., 2021; Kocher, 2004; Powder and Albertson, 2016; Roberts et al., 2009).

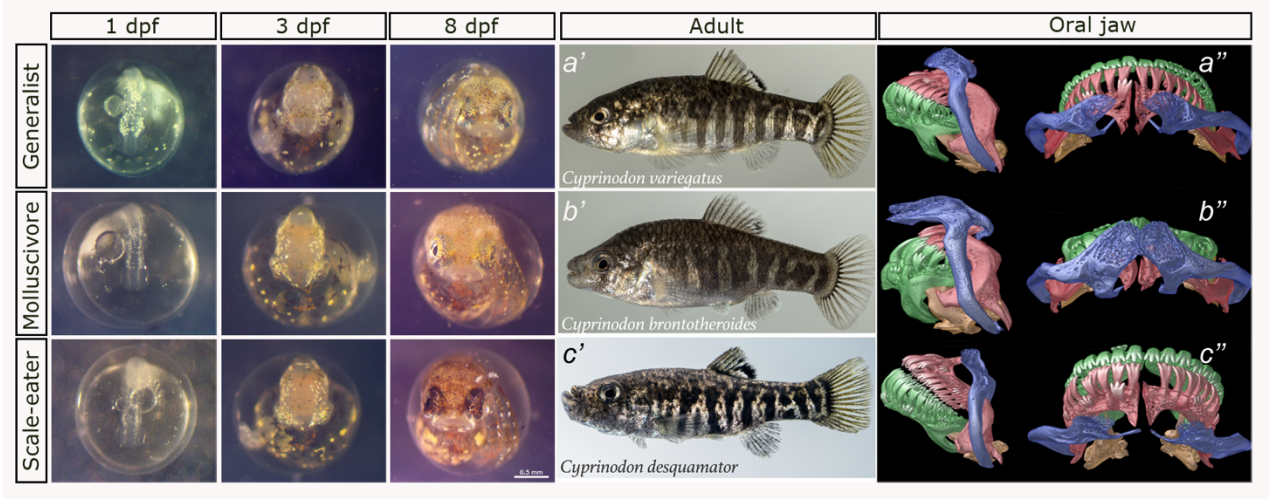

Figure 1. Divergent craniofacial morphology and development of the San Salvador Island *Cyprinodon* pupfish radiation. *C. variegatus* (first row) is a trophic generalist distributed across the western Atlantic and Caribbean; *C. brontotheroides* (second row) is a molluscivore, and *C. desquamator* (third row) is a scale-eater, both endemic to the hypersaline lakes of San Salvador Island (SSI), Bahamas. Left panel: development at 1-, 3-, and 8-days post-fertilization (dpf). Middle panel: lab-reared adult female pupfishes of each species. Right panel: Lateral and dorsal views of μCT scans of craniofacial morphology (modified from Hernández et al., 2017). The maxilla is colored in blue, premaxilla in red, dentary in green, articular in orange.

Here we demonstrate the utility of a non-model evolutionary radiation of *Cyprinodon* pupfishes for discovering and validating a new craniofacial gene of potential clinical relevance to normal human facial variation and craniofacial disorders. Pupfishes offer unique advantages over other evolutionary model systems because they 1) rapidly evolved highly divergent and unique craniofacial phenotypes not found in other non-model fish systems (Fig. 1) with minimal genetic differentiation among species (Hernandez et al., 2018; Lencer et al., 2016; Lencer et al., 2017; Martin and Wainwright, 2011; Martin and Wainwright, 2013a; Martin et al., 2019; St John et al., 2020a; St John et al., 2020b), 2) speciated in the face of ongoing gene flow after colonizing hypersaline lakes, resulting in very few highly differentiated genomic regions associated with

111 species-characteristic craniofacial traits (Martin and Feinstein 2014; Martin et al., 2017; McGirr
112 and Martin, 2016; McGirr and Martin, 2021; Richards and Martin, 2017; Richards and Martin,
113 2022; Richards et al., 2021), and 3) are highly amenable to laboratory rearing and imaging due to
114 their high fecundity, daily egg production, and egg transparency comparable to zebrafish (Martin
115 and Gould, 2020; Martin and Wainwright, 2013b). This radiation contains the widespread algae-
116 eating generalist pupfish, *Cyprinodon variegatus* (Fig. 1a), which is broadly distributed across the
117 Caribbean and North American Atlantic coast and occurs in sympatry with two microendemic
118 trophic specialist species found only in the hypersaline lakes of San Salvador Island (SSI),
119 Bahamas. Each trophic specialist displays highly divergent behavior, pigmentation, and
120 craniofacial morphology: the molluscivore *C. brontotheroides*, has a novel nasal protrusion that is
121 a skeletal extension of the maxilla with bilateral nasal tissue clefting and foreshortened robust oral
122 jaw (Fig. 1b); and the scale-eater, *C. desquamator*, exhibits two-fold larger oral jaws and overall
123 brachycephalic features (Fig. 1c) (Martin, 2016; Martin and Wainwright, 2011; Martin and
124 Wainwright, 2013a). There is also a fourth intermediate scale-eating ecotype in some lakes
125 (Richards et al. 2022).

126 Previous genomic and transcriptomic work on the SSI pupfishes identified dozens of new
127 candidate craniofacial genes never previously characterized or investigated in other systems
128 (McGirr and Martin 2016, 2019, 2020; Richards et al. 2021, 2022; Richards and Martin 2017;
129 Patton et al. 2021; St. John et al. 2021). One of the most promising candidates was galanin receptor
130 2a, the second receptor type for galanin (see discussion of genomic evidence in Methods and
131 Materials). In humans, *galr2* is abundantly expressed within the hypothalamus and hippocampus
132 of the central nervous system and in the heart, kidney, liver, colon, and small intestine, and has
133 genetic associations with epilepsy and Alzheimer's (Li et al., 2013; Ma et al., 2018). Classified as

134 an orexigenic (appetite stimulant) gene, *galr2* is expressed in the human hypothalamus but also in
135 the ventral telencephalon of larval and adult zebrafish (Ahi et al., 2019; Li et al., 2013; Kim et al.,
136 2016). Although a role of *galr2* in craniofacial development has not previously been reported in
137 the literature, its ligand, the neuropeptide galanin (GAL), is highly expressed in bones from early
138 to post-embryonic development (Xu et al., 1996, Jones et al., 2009), with demonstrated effects on
139 bone mass (Idelevich et al., 2018; Idelevich et al., 2019), muscle contraction (Kakuyama et al.,
140 1997. EJP), and periodontal regeneration (Ma et al. 2021).

141 Here we confirmed the presence of two highly differentiated SNPs between SSI specialist
142 species affecting transcription factor binding sites in the *galr2* regulatory region, characterized the
143 divergent craniofacial expression of *galr2* across all three SSI pupfish species from two different
144 lake populations using *in situ* hybridization chain reaction (HCR) (Choi et al., 2018; Ibarra-Padilla-
145 García et al., 2020) at two key developmental timepoints, and demonstrated that receptor inhibition
146 of exclusively the Galr2 pathway reduces Meckel's cartilage length and increases chondrocyte
147 density dependent on the species' genetic backgrounds.

148

149 **Results**

150 **Two highly differentiated SNPs are associated with *galr2a* transcription factor binding sites**

151 Previous whole genome sequencing of over one hundred San Salvador Island (SSI) pupfishes
152 identified only two single nucleotide polymorphisms (SNP) nearly fixed between trophic
153 specialists across lake populations within 20 kb of *galr2a* (Richards et al. 2021). We designed
154 primers and used Sanger sequencing to verify these SNPs in a large panel of wild-caught specialists
155 from five lake populations on SSI (Table S5). We confirmed the presence of a transversion from
156 G to A approximately 11 kb upstream of the *galr2a* transcription starting site (TSS; Fig. 2a., S1;

157 Table S1), which changes the predicted CA**G**CAA *Elf1/Erg* transcription factor binding site
158 (TFBS) to an **A**GGGASW *Elf5* TFBS at this locus (using the Multiple Expectation maximizations
159 for Motif Elicitation (MEME) server and the motif database scanning algorithm TOMTOM
160 (Bailey et al., 2009)). This transversion was observed in 86.3% of scale-eaters across four lake
161 populations (n = 51) versus 20% of molluscivores across six lake populations on SSI (n = 30) (Fig.
162 2a., S1).

163 We confirmed the presence of a second transversion from C to T approximately 8 kb
164 upstream of *galr2a* TSS, which changes the predicted AGA**C**AA *Sry* TFBS to a YAGA**T**A *Znf146*
165 TFBS (Fig. 2b., S2; Table S1). This transversion was observed in 90.9% of scale-eaters across four
166 lake populations (n = 55) versus 33.9% of molluscivores across six lake populations on SSI (n =
167 53) (Figure S2). Notably, all scale-eaters sampled from Crescent Pond (CRP) contained the T
168 transversion (n = 30) (Supplementary Figure S3). The predicted TFBS changes in the *galr2a* cis-
169 regulatory region across pupfishes, combining with a previous genetic mapping study that found
170 a significant QTL in this region explaining 15% of phenotypic variance in oral jaw size (Martin et
171 al. 2017), suggests that different spatial or temporal *galr2* expression may underlie some of the
172 craniofacial divergence in SSI pupfishes.

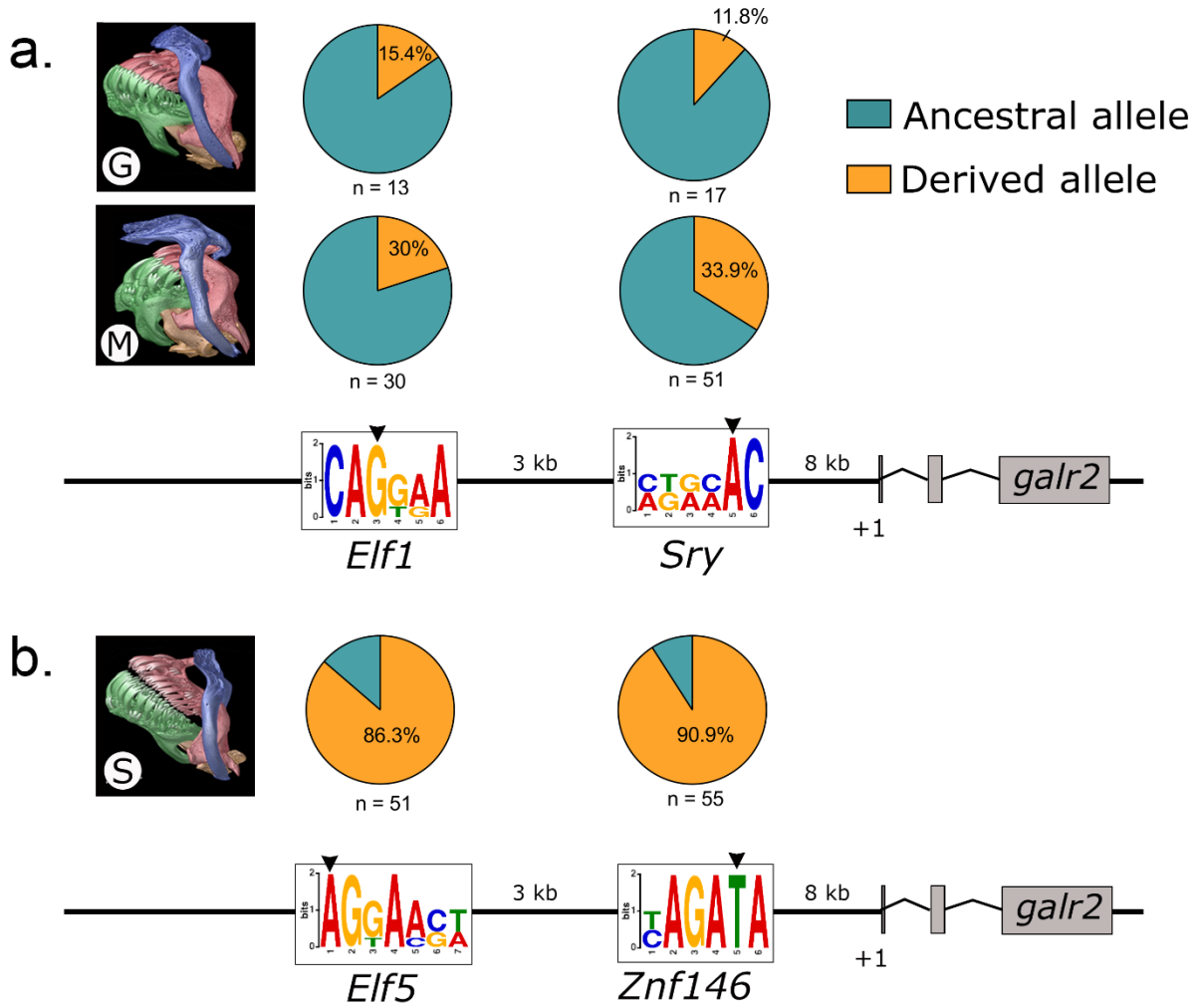

Figure 2. The two most differentiated single-nucleotide polymorphisms (SNP) between trophic specialists within 20kb upstream of *galr2*. a. Putative ancestral TFBS for *Elf1/Erg* and *Sry*, respectively, in the generalist (G), *Cyprinodon variegatus* and the molluscivore (M) *Cyprinodon brontotheroides*. **b.** Derived changes in TFBS to *Elf5* and *Znf146* in the scale-eater (S) *Cyprinodon desquamator*. Pie charts indicate frequencies of ancestral (teal) and derived (orange) alleles at each locus. +1 represents the transcription starting site of *Galr2a* (Galanin receptor 2a). µCT scans of craniofacial morphology are modified from Hernández et al., 2017. Sequence logos of the Position Weight Matrixes (PWM) identified using MEME and TOMTOM.

184 **Different spatiotemporal patterns of *galr2a* expression in craniofacial tissues**

185 To determine if spatial or temporal changes in *galr2a* expression underlie SSI craniofacial
186 divergence, we quantified *galr2a* expression in 2 dpf embryos and 8 dpf hatching larvae across all
187 SSI species in two independent lake populations using hybridization chain reaction (HCR) in-situ
188 hybridization for *galr2a* and *tropomyosin 3b* (*tpm3b*), a component of thin filaments of myofibrils
189 expressed in fish skeletal muscles (Dube et al., 2016), as a positive control.

190 At 2 dpf, *galr2a* was expressed in more regions of the central nervous system of specialists
191 (Fig. 3a,c) than in generalists (e.g. the posterior tectum and medial longitudinal fasciculus);
192 however, we observed increased *galr2a* expression in the first pharyngeal arches and the
193 surrounding mandibular mesenchyme in the molluscivore and generalists pupfishes than in the
194 scale-eaters. In addition to an absence of *galr2a* expression in the mesenchyme surrounding the
195 first pharyngeal arch, its expression was conserved in the first and second pharyngeal arches and
196 clefts (Fig. 3c,e).

197 Using 3D reconstruction and volume rendering analysis of HCR data for whole-mounted
198 pupfishes at hatching time (8 dpf), we found that *galr2a* expression was higher in the jaw of the
199 molluscivores than in the generalists (Fig. 4; $P = 0.03$, Tukey's HSD). In contrast, *galr2a* showed
200 no differences in expression among species in the brain and head (Fig. 4, Table S3). G*alr2a* was
201 expressed in the Meckel's and palatoquadrate cartilages in all SSI pupfishes, in the premaxilla of
202 the generalist and the scale-eater SSI specialist (Fig. 4 b-b', c-c'), the maxilla of the molluscivore
203 SSI specialist (Fig. 4 a-a'), and in the intermandibular muscles of the scale-eaters (Fig. 4 c').

204 At the subcellular level, *galr2a* was expressed in the cytoplasm of chondrocytes at the
205 Meckel's symphysis (Fig. 5a). In contrast, on the distal edge of the Meckel's cartilage it was
206 expressed only in the cytoplasm of the elongated chondrocytes (Fig. 5a'). Towards the most

207 posterior region of the Meckel's closest to the palatoquadrate cartilage, we observed strong
208 membrane expression of *galr2a* in the cells surrounding the jaw joint (Fig. 5 b, c, d). We conclude
209 that g*alr2a* was significantly differentially expressed in specific and distinct craniofacial tissues in
210 the specialists at hatching time, suggesting an important role for craniofacial divergence in the SSI
211 radiation.

212 We further corroborated the differential spatial expression of *galr2a* at 2 dpf and 8 dpf by
213 quantifying transcript counts from the only existing RNAseq data set on SSI heads during
214 development (Lencer and McCune, 2020). Only *galr2a*, but not *galr1a, galr1b, galr2a, galr2b,* or
215 *galanin*, showed significantly higher mRNA expression in the molluscivores relative to generalists
216 (P = 0.003, Tukey's HSD test) and scale-eaters (P = 0.014, Tukey's HSD test) at 2 dpf (Table S2),
217 whereas *galr2a* showed overall similar levels of expression in the head from 4 to 15 dpf in all three
218 species (Table S2).

219 As the rapid evolution of jaw size in the SSI radiation is accompanied by rapid divergence
220 of the adductor muscle mass (Martin and Wainwright, 2011) and hypertrophy of the adductor
221 mandibulae complex (Hernandez et al., 2018), we selected a known skeletal muscle gene, *tpm3b*
222 (tropomyosin alpha-3) as a positive control for our HCR and to test for possible muscle differences
223 between species during jaw development. At 2 dpf that *tpm3b* was expressed in adaxial cells, the
224 first muscle precursor cells, in all SSI pupfishes (Fig. 3a''-c''). However, only in the scale-eaters,
225 *Tpm3b* was expressed in the eye's inferior oblique muscle primordial cells (Fig. 3c''). At hatching
226 time, *Tpm3b* labeled all larval head muscles (Fig. 4a-a', b-b', c-c'; 5b). The scale-eater and
227 molluscivore *Tpm3b* expression volume was significantly higher than in the generalists (Table S3;
228 P < 0.05; 1-way ANOVA, Tukey's HSD test).

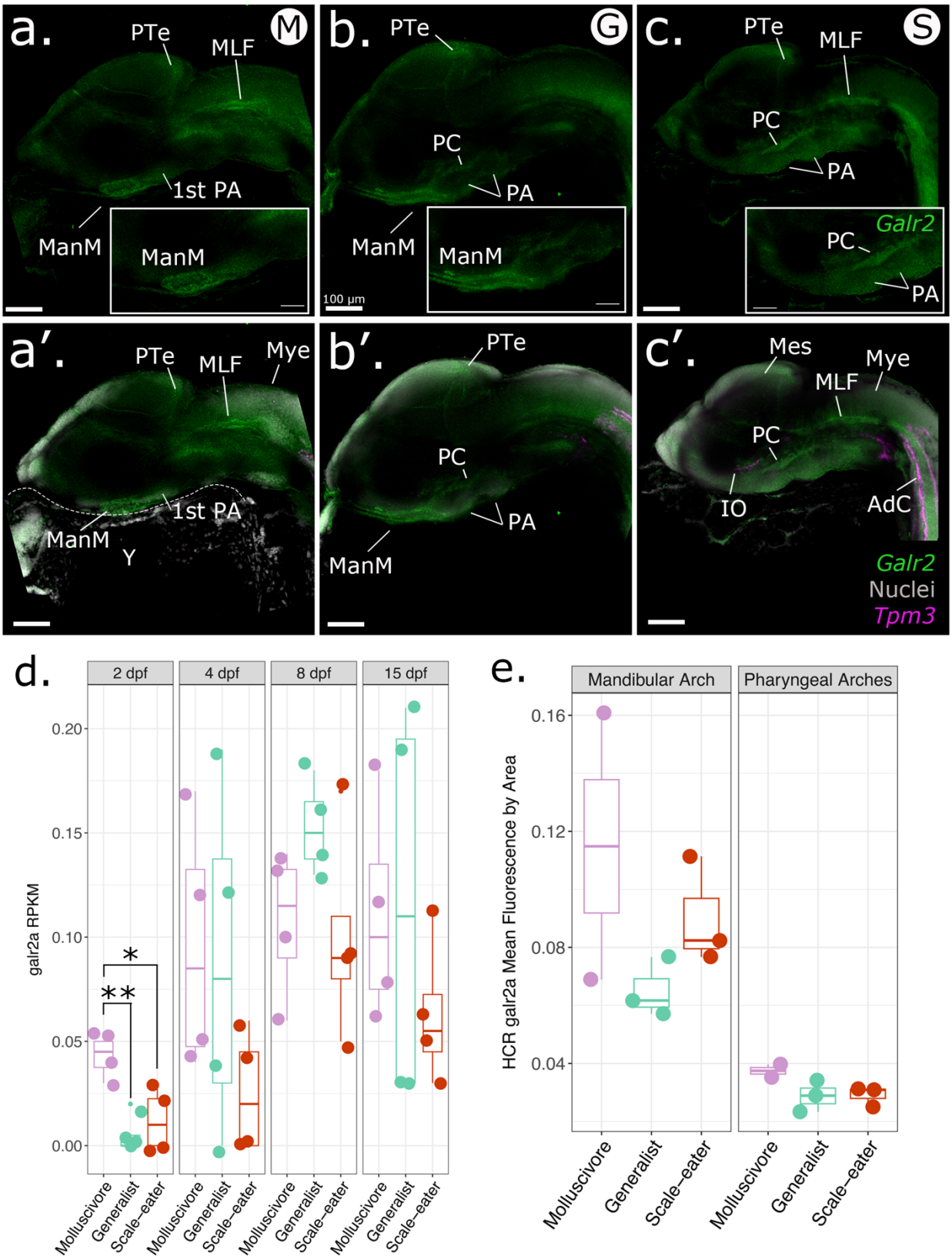

229 **Figure 3. Spatiotemporal patterns of *galr2a* expression differ among SSI species at 2 dpf.**

230 Representative images of *Galr2a* (green) and *Tpm3b* (magenta) expression revealed by hybridization chain

231 reaction (HCR) and DAPI nuclear staining (gray) in the: **a.** molluscivore, *C. brontotheroides*; **b.** generalist,
232 *C. variegatus*; and **c.** scale-eater, *C. desquamator*. **d.** Galr2a reads per kilobase of transcript per million
233 reads (RPKM) from an existing mRNAseq study sampling the entire head of each species at four
234 developmental stages (Lencer and McCune, 2020). Galr2a showed significantly higher expression in the
235 molluscivore relative to generalists (P = 0.003, Tukey's HSD test) and scale-eaters (P = 0.014, Tukey's
236 HSD test) at 2 post fertilization (dpf). **e.** Mean fluorescence per area for galr2a quantified at 2 dpf in all three
237 species shows similar elevated levels of expression in the molluscivore for the mandibular and pharyngeal
238 arches. Images shown are representative Z-stack maximum projection images of 30 optical sections taken
239 every 15 μm from whole-mounted larvae imaged using a Zeiss LSM880 laser confocal microscope. PA:
240 pharyngeal arches, PC: pharyngeal cleft, ManM: mandibular mesenchyme, MLF: medial longitudinal
241 fasciculus, PTe: posterior tectum, Di: diencephalon; Mes: mesencephalon, Mye: myelencephalon, Y: yolk,
242 AdC: Adaxial cells, IO: inferior oblique muscle.

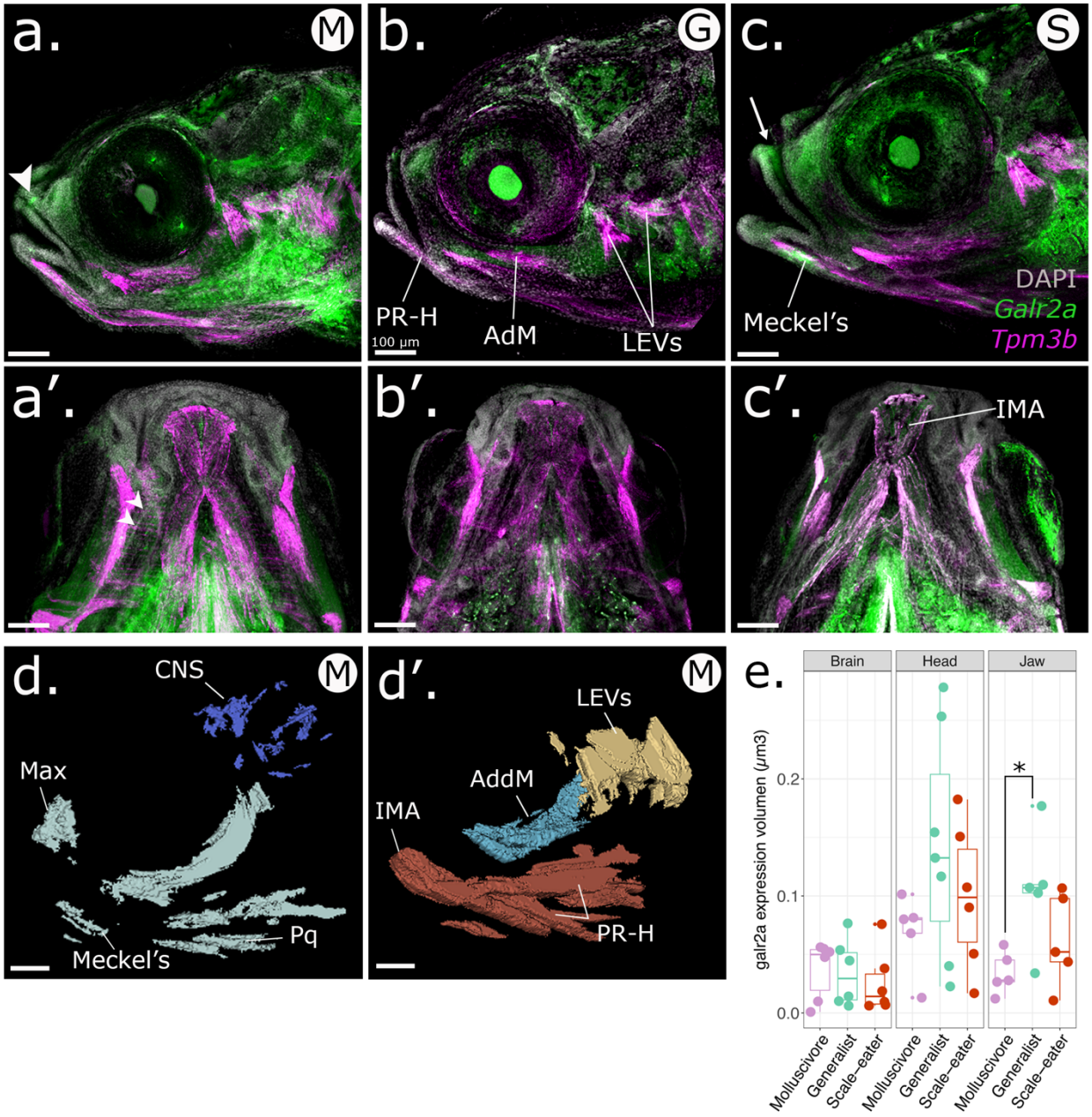

Figure 4. Spatiotemporal patterns of *galr2a* expression differ in molluscivores at 8 dpf. Representative images of *Galr2a* (green) and *Tpm3b* (magenta) expression revealed by hybridization chain reaction (HCR) and DAPI nuclear staining (gray). **a.** Lateral view of an 8 dpf molluscivore (M in white circle), **a'.** ventral view. **b.** Lateral view of an 8 dpf generalist (G in white circle), **b'.** ventral view. **c.** Lateral view of an 8 dpf scale-eater (S in white circle), **c'.** ventral view. The arrowhead in **b.** and the arrow in **c.** point to high expression of *galr2a* in the maxilla and premaxilla of the molluscivore and scale-eater specialists, respectively. White arrowheads in **a'.** point to high expression of *galr2a* in the palatoquadrate of the

250 molluscivore. Images shown here are representative Z-stack maximum projection images of 30 optical
251 sections taken every 15 µm from whole-mounted larvae imaged using a Zeiss LSM880 laser confocal
252 microscope. **d-d'.** 3D-Slicer view of the expression volume of *galr2a* (**d.**) and *tpm3b* (**d'.**) in a hatched
253 molluscivore pupfish larvae (*C. brontotheroides*). **e.** Volume of *galr2a* expression in the brain (left panel),
254 whole head (middle panel), and jaw (right panel) across SSI pupfishes. CNS: central nervous system, Max:
255 maxilla. LEVs: levator arcus palatini and operculi, AdM: adductor mandibular. IMA: intermandibular anterior.
256 Total volume rendered: 450 µm. All scale bars: 100 µm.

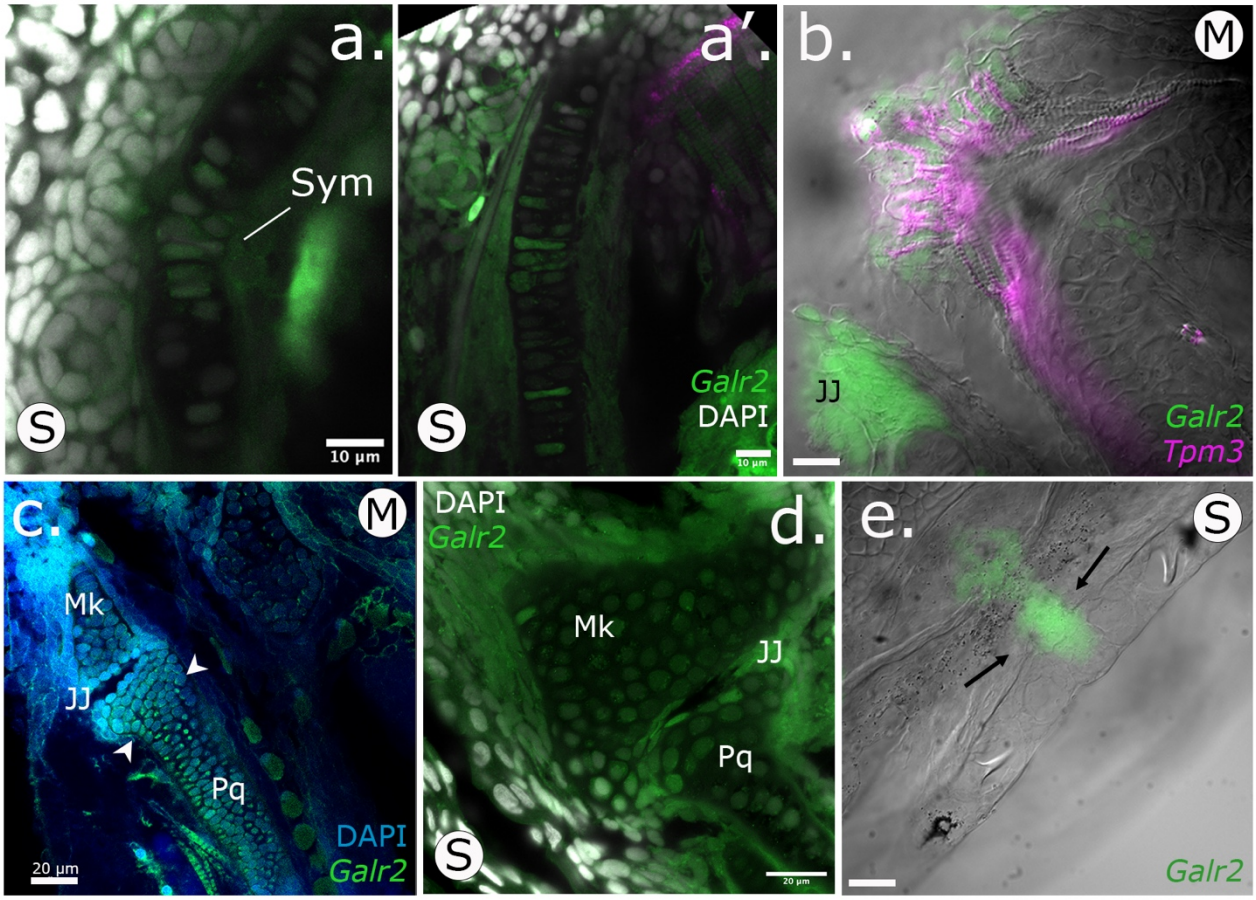

257 **Figure 5. *Galr2a* is expressed in the chondrocytes of the Meckel's and palatoquadrate cartilages at**
258 **hatching (8 dpf) in SSI pupfishes.** HCRs showing tissue expression of *Galr2a* in green, and the muscle
259 marker Tropomyosin 3b, (*Tpm3b*), in magenta. Nuclei are stained with DAPI (gray). **a-a'.** Scale-eater *galr2a*
260 expression in the chondrocytes of the Meckel's symphysis (Sym) and lateral side. **b.** Ventral view of a
261 molluscivore jaw at 8 dpf showing the expression of *Tpm3b* in the intermandibular muscles of the lower
262 jaw. *Galr2a* is expressed in the jaw joint and the most anterior region of the lower jaw. **c-d.** *Galr2a* is

263 expressed in the chondrocytes of the Meckel's and palatoquadrate cartilages and around the jaw joint. **e.**
264 *Galr2a* expression in the premaxilla of a scale-eater. Unlabeled scale-bars: 10 μm.
265

266 **Chemical inhibition of Galr2 receptors affects Meckel's cartilage length and chondrocyte**
267 **density**

268 To study the effect of Galr2 in craniofacial development, we inhibited the endogenous activation
269 of all four known galanin receptors in teleost fishes (*Galr1a* and b, *Galr2a* and b; Butler et al.
270 2020, Li et al. 2013) using M35 (Innopep, Inc.), a synthetic peptide antagonist of Galr1+2 galanin
271 receptors (Wiesenfeld-Hallin et al., 1993), and M871 (Abcam), a Galr2-specific synthetic peptide
272 antagonist (Sollenberg et al., 2006). Embryos of all three species from two different lake
273 populations were exposed from stages 24-25 (2 dpf, with the appearance of the first pharyngeal
274 arches) until hatching at stages 32-33 (8 dpf, Fig. 6a).

275 At approximate hatching time (8 dpf), both trophic specialist species raised under
276 laboratory common garden conditions exhibited increased Meckel's cartilage length (Fig. 6d),
277 consistent with the longer jaws of adult scale-eaters and more robust jaws of the molluscivore
278 relative to more gracile jaws of the generalist (Martin and Wainwright 2013). We found that
279 exposure to M871, the Galr2-specific antagonist, significantly reduced the length of the Meckel's
280 cartilage in both specialists relative to the generalists (Fig. 6d.; $P = 7.89 \times 10^{-5}$ for scale-eaters; P
281 = 0.001 for molluscivores; 2-way ANOVA, Tukey's HSD test). In contrast, M35 (Galr1 and Galr2
282 antagonist) only significantly reduced Meckel's length in the molluscivore (Fig. 6c). Meckel's
283 length of generalists was unaffected by exposure to M35 or M871 (Fig. 6d).

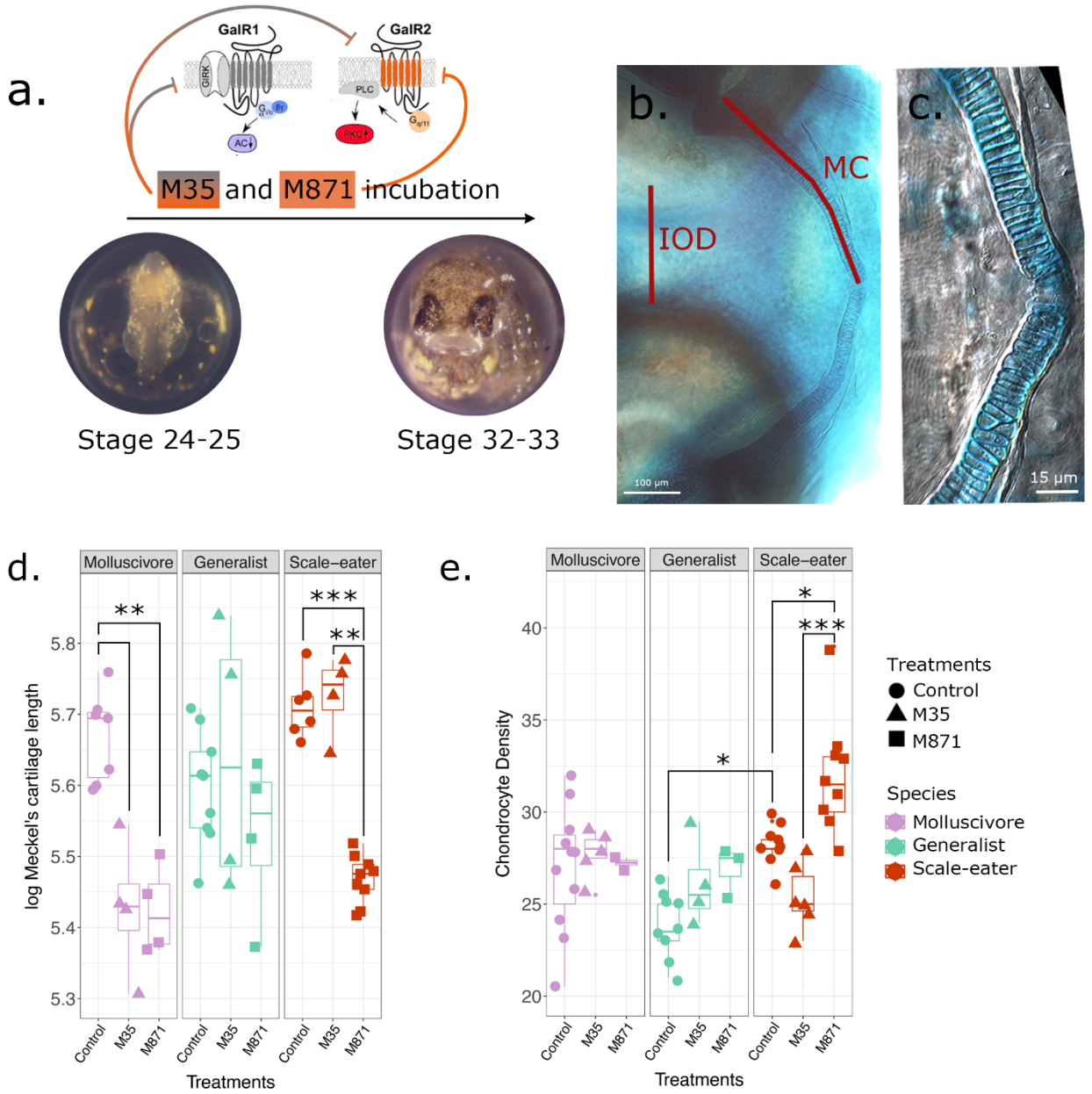

Figure 6. Galr2 receptor inhibition reduced Meckel's cartilage length in both specialists and increased chondrocyte density in scale-eaters. a. Galr2 and Galr1+2 inhibition protocol during pupfish development. *C. desquamator* embryos are depicted. **b.** Alcian blue cartilage staining at Stage 32-33. IOD: interocular distance, MC: Meckel's cartilage. The MC length and IOD are shown in red. **c.** Chondrocytes at the symphysis. **d.** Changes in the log-transformed Meckel's length and the log-transformed interocular distance at Stage 32-33 across species and treatments. **e.** Chondrocyte numbers at the symphysis across species and treatments. *$P < 0.05$, **$P < 0.01$, ***$P < 0.001$ Tukey's HSD test.

292 To understand the cellular effect of Galr1 and 2 antagonists on Meckel's length across
293 species, we quantified the number of chondrocytes 100 μm from the symphysis and the mean
294 width of ten chondrocytes nearest to the symphysis. We found no significant differences in the
295 mean chondrocyte width among pupfish species but observed increased chondrocyte density in
296 untreated scale-eaters relative to generalists (Fig. 6e; Table S4; P = 0.009, ANOVA, Tukey's HSD
297 test). Moreover, only scale-eaters responded to M871, but not M35, by further increasing
298 chondrocyte density relative to the control larvae (Fig. 6e; Table S4; P = 0.03, ANOVA, Tukey's
299 HSD test; mean ± 1 SE; control = 28.22 ± 0.38; M871 = 32.06 ± 1.06). Despite having shorter
300 jaws after treatment with M871, chondrocyte density was significantly increased (Fig. 6e; mean ±
301 1 SE; control = 28.22 ± 0.38; M871 = 32.06 ± 1.06).
302
303 **Discussion**
304 We used a non-model evolutionary radiation of trophic specialist pupfishes, endemic to the
305 Bahamas, to discover a novel function for *galr2a* in craniofacial divergence. Specifically, we
306 confirmed that only two transcription factor binding sites upstream of *galr2a* display highly
307 divergent allele frequencies between trophic specialist species, visualized *galr2a* expression in
308 craniofacial tissues in all three SSI pupfish species at two developmental stages, and demonstrated
309 a phenotypic effect on Meckel's cartilage length and chondrocyte density using synthetic peptides
310 to inhibit the activity of Galr2 and Galr1+2. Our findings demonstrate a crucial role for Galr2 in
311 craniofacial divergence within this pupfish radiation. Our study also provides a roadmap in a non-
312 model vertebrate system for rapidly identifying previously uncharacterized candidate genes
313 important for adaptation to novel ecological niches (e.g. trophic specialization) that can be quickly
314 validated through classic and state-of-the-art developmental biology tools. Overall, our research

315 contributes to understanding the genetic basis of phenotypic evolution and adaptation in non-
316 model organisms.
317
318 **Putative loss of a transcription factor binding site for *galr2a* in scale-eating pupfish**
319 One of the most common evolutionary changes associated with phenotypic changes among closely
320 related species is the gain or loss of cis-regulatory elements (Mack and Nachman, 2017; Signor
321 and Nuzhdin, 2018). More than 85% of scale-eaters carry two transversions in the regulatory
322 region of *galr2a* (Fig. 2). Combined with our observations of reduced *galr2a* expression in the
323 mandibular mesenchyme during early jaw development in this species (Fig. 3), we conclude that
324 a loss of a Sry transcription factor binding site in scale-eaters is the most likely explanation for
325 changes in gene expression, rather than a gain of a new TFBS for Znf416 at this locus (Fig. 2).
326 This is further supported by the critical role of the Sry-related HMG box (Sox) family of
327 transcription factors (especially the SoxE group including Sox8, Sox9, and Sox10) in craniofacial
328 development as Sry transcription factors specify the behavior, multipotency, and survival of neural
329 crest cells during vertebrate development (Leathers and Rogers, 2022; Simões-Costa and Bronner,
330 2015; Guo et al., 2015; Haldin and LaBonne, 2010; Betancur et al., 2010; Kamachi and Kondoh
331 2013).
332 Alternatively, we cannot rule out a gain of a TFBS upstream of *galr2a* in scale-eaters,
333 additive or epistatic effects of both upstream inversions, or more complex regulatory architectures,
334 such as many interacting functional cis- and trans-acting regulatory variants or combinations of
335 variants segregating at lower frequencies in trophic specialists that we have not prioritized (Boyle
336 et al., 2017; McGirr and Martin, 2021; Price et al., 2015). However, our mapping cross of a single
337 outbred pair of trophic specialists indicates that a single moderate-effect QTL containing *galr2a*

338 explains 15% of phenotypic variation in oral jaw length between these species, consistent with
339 causative variants affecting jaw size originating from this region (Martin et al. 2017).
340

341 **Differential *Galr2a* expression during development is associated with craniofacial divergence**
342 **in SSI pupfishes**

343 We found *galr2a* expression in our in situ hybridization experiments to be consistent with
344 previously published RNAseq data for craniofacial tissue in this radiation (Fig. 3; Lencer and
345 McCune, 2017). We observed distinctive spatial *galr2a* expression among SSI species at 2 and 8
346 dpf suggesting important time and tissue-specific regulation of *galr2a* expression during pupfish
347 development. At 2 dpf, we found a strong association between decreased expression of *galr2a* in
348 the mandibular mesenchyme anterior to the first pharyngeal arch with the future Meckel's cartilage
349 and oral jaw lengths in the adults of each species; with increasing *galr2* abundance in the
350 molluscivores associated with shorter, but more robust jaws in adults (Martin and Wainwright
351 2013). In contrast, the reduced *galr2a* expression in the mandibular mesenchyme is associated
352 with the development of longer oral jaws in scale-eaters, which is apparent as early as hatching
353 time (Fig. 6d; Lencer et al., 2016).

354 We noted expression of *galr2a* in the maxilla of only molluscivores at hatching (Fig. 4 a-
355 c), absent in the scale-eaters and generalists, consistent with the uniquely enlarged and anteriorly
356 protruding head of the maxilla in this species (Martin and Wainwright 2013; Hernandez et al. 2018;
357 Martin and Feinstein 2014; St. John et al. 2020). Furthermore, *galr2a* expression in the
358 intermandibular muscles of the scale-eaters at hatching time is consistent with the observed
359 hypertrophic musculature of the adductor mandibulae in the adult scale-eating pupfish (Hernandez
360 et al., 2018). Altogether, these interspecific differences in spatial expression support a novel role

361 for *galr2a* in musculoskeletal development accounting for the divergent craniofacial morphology
362 observed in SSI pupfishes.
363
364 **Receptor inhibition reveals a novel function for GALR2 in craniofacial divergence of SSI**
365 **pupfishes**
366 Interestingly, the response of Meckel's cartilage length and chondrocyte density to the inhibition
367 of Galr-receptor pathways was highly dependent on the species' genetic background. Scale-eaters
368 responded only to the Galr2-specific antagonist M871 with substantially reduced Meckel's
369 cartilage length and increased chondrocyte density, but were unaffected by the Galr1+2 antagonist
370 M35 (Fig. 6c). Importantly, M871 exhibits a higher binding constant for Galr2 receptors than the
371 Galr1+2 antagonist M35 (Sollenberg et al., 2006; Sollenberg et al., 2010). Previous transcriptomic
372 data from craniofacial tissues during early development (Lencer and McCune 2017) also indicates
373 that *galanin* and *Galr1* mRNA transcript abundance does not vary among the three SSI species
374 (Table S3).
375 Therefore, we conclude that even though scale-eaters expressed the lowest amount of *galr2a*
376 transcripts and presumably contain overall fewer Galr2 receptors in their craniofacial tissue,
377 M871's higher binding affinity was sufficient to inhibit these fewer receptors, resulting in reduced
378 Meckel's cartilage length (Fig. 7). In contrast, the presumably greater concentration of Galr2
379 receptors in molluscivore craniofacial tissue due to increased Galr2 expression during
380 development resulted in the inhibition of these receptors by both M871 and M35, despite its lower
381 binding affinity for Galr2 (Lang et al., 2007). We also conclude that inhibition of Galr1 receptors
382 by M35 does not affect Meckel's cartilage length or chondrocyte density and that the specific
383 inhibition of Galr2 by M871 was sufficient to drive equal Meckel's cartilage length shortening.

384 Finally, the generalists' lack of significant response to M35 is consistent with their decreased levels
385 of *galr2a* at 2 dpf, suggesting that, as in scale-eaters treated with M35, fewer Galr2 receptors may
386 be present for inhibition in these species' background. However, the response to M871 appears to
387 be specialist-specific, with little effect on the generalist Meckel's cartilage length, and thus, we
388 cannot rule out more complex species-specific factors interacting with Galr regulatory pathways.

389 Our work is consistent with previous work showing that *Galr2* activation inhibits cell
390 proliferation in neuronal cell lines (Lang et al., 2007; Berger et al., 2004), suggesting that the TFBS
391 allele frequency shifts observed in scale-eaters causing low *galr2a* abundance and, as a
392 consequence, have low Galr2 activity during craniofacial development, result in the increased
393 chondrocyte density and Meckel's cartilage length observed in scale-eaters. Thus, the increased
394 chondrocyte density observed in the M871-treated scale-eater larvae results likely from the strong
395 and continued inhibition of fewer Galr2 available during development as a consequence or a
396 synergy of/with their genetic background.

397 In conclusion, we propose that the inhibition of Galr2 and not Galr1 induces the reduction
398 of Meckel's cartilage length. Thus, a greater number of Galr2 receptors in the molluscivore
399 specialist, as a result of increased expression of *galr2a* during early development, may result in
400 their reduced oral jaw lengths as adults through increased opportunities for endogenous agonistic
401 binding interactions (Fig. 7). Fewer Galr2 receptors on the scale-eater jaw may result in their
402 enlarged jaw lengths as adults by limiting opportunities for Galr2 endogenous agonists to bind to
403 these receptors during development. In the generalists, a greater number of Galr2 receptors but
404 smaller overall Meckel's cartilage length may limit the sensitivity of this species to Galr2 and
405 Galr1+2 endogenous agonists, however, resulting in their intermediate length and least robust oral

406 jaws among the three species under control conditions (Hernandez et al. 2018; Martin and
407 Wainwright 2011).

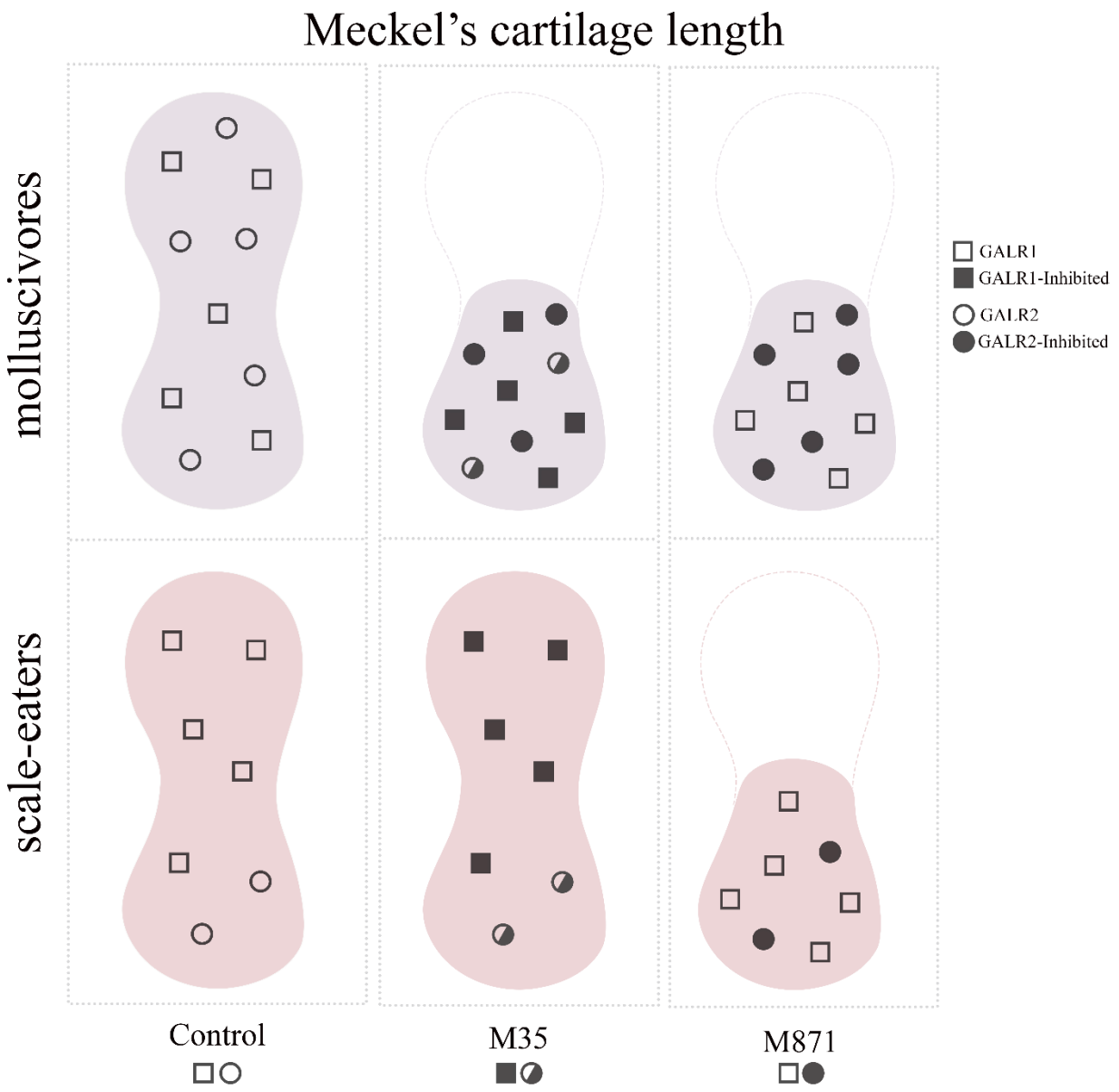

408

409 **Figure 7. Proposed mechanism for how galanin receptor abundance affects Meckel's cartilage**
410 **length in the two pupfish trophic specialists after exposure to M35 (weak Galr1+Galr2 antagonist)**
411 **or M871 (strong Galr2 antagonist).** Molluscivores (top row) express more *galr2a* at 2 and 8 dpf than scale-
412 eaters (bottom row) in their Meckel's cartilage (see Figs. 3-4), resulting in more Galr2 receptors (open
413 circles). Increased Galr2 receptor density in molluscivores results in their reduced Meckel's cartilage length

414 (see Fig. 6) due to inhibition by both the weak antagonist (M35: middle column; half-filled circles) and strong
415 antagonist (M871: right column; filled circles) of Galr2. In contrast, reduced Galr2 receptor density in scale-
416 eaters (bottom row) results in their reduced Meckel's cartilage length only after exposure to the strong
417 Galr2-specific antagonist M871.
418

419 **Conclusion**

420 Our results show a novel role of the second receptor for galanin, Galr2, as a craniofacial gene
421 important in controlling craniofacial development and interspecific divergence through modifying
422 its transcript abundance and receptor activity. *Galr2a* transcript abundance changes are associated
423 with genetic changes in the regulatory region of *galr2a*, consistent with the loss of a transcription
424 factor binding site in the scale-eating pupfish. We propose a model in which reduced Galr2
425 receptor density in the oral jaws of scale-eaters results in fewer endogenous agonistic interactions,
426 increasing Meckel's cartilage length presumably by decreased inhibition of chondrocyte
427 proliferation (as a downstream effect of endogenous Galr2 activation). We also acknowledge the
428 polygenic nature of jaw development and note that our previous genetic mapping experiments
429 place an upper bound of 15% of oral jaw variation that may be due to differences in *galr2a*
430 regulation among the myriad craniofacial genes driving the evolution of divergent craniofacial
431 traits in this system.
432

433 **Materials and Methods**

434 ***Genomic evidence for galr2 as a candidate craniofacial gene***

435 Using a genome-wide association (GWA) test across 202 individuals from the SSI radiation and
436 outgroup populations, we previously found an association of the regulatory region of *galr2a* with
437 lower jaw length, confirming an earlier pilot study that found the *galr2a* region to be among the

438 top five strongest associations with lower jaw length containing highly differentiated SNPs
439 between trophic specialist species (Richards et al. 2021; McGirr and Martin 2017). An analysis of
440 hard selective sweeps using both site frequency spectrum (SweeD) and linkage disequilibrium
441 (Omegle) based summary statistics additionally found evidence of a putative adaptive allele in the
442 20 kb regulatory region upstream of *galr2* (Pavlidis et al., 2013; Richards et al., 2021). This allele
443 swept to fixation in the scale-eater *C. desquamator* population on SSI 696-1,008 (95% credible
444 interval) years ago, potentially providing a pivotal stage in adaptation to scale-eating (Richards et
445 al. 2021). An independent quantitative trait loci (QTL) mapping study in F2 intercross hybrids
446 between scale-eater and molluscivore parents found a significant QTL on linkage group 15
447 containing *galr2a* that accounted for 15.3% of the phenotypic variance in premaxilla length (n =
448 178; Martin et al. 2016). Similarly, a second independent study of F2 intercross hybrids from a
449 second lake found evidence of a QTL in this region explaining 8% of the phenotypic variance in
450 the length of the coronoid process on the articular bone of the lower jaw (jaw closing in-lever; n =
451 227; St. John et al. 2021). The combined strength of evidence for a role of *galr2a* in craniofacial
452 development across independent analyses of GWA, QTL, selective sweeps, and genetic
453 differentiation between species indicated that this was one of our highest priority candidates for
454 functional studies.
455
456 **Pupfish husbandry and maintenance**
457 Three sympatric *Cyprinodon* species (*C. variegatus, C. bronthotheroides,* and *C. desquamator*)
458 were collected from both Osprey Lake and Crescent Pond in San Salvador Island, Bahamas in
459 2018 and maintained in the lab for at least two generations in small breeding groups. All lab
460 colonies were maintained at a pH of 8.0 and 2-5 ppt salinity at 25-30°C on a 12:12 hours light:dark

461 cycle at the University of California, Berkeley. Newly hatched fry were raised on brine shrimp
462 nauplii for the first month and adults and juveniles were fed a combination of commercial pellet
463 food and frozen bloodworms. All protocols and procedures employed were reviewed and approved
464 by the University of California, Berkeley Animal Care and Use Committee (AUP-2015-01-7053)
465 and animals were collected and exported from the Bahamas with research and export permits from
466 the Bahamas Environmental, Science, and Technology commission through the Gerace Research
467 Centre.

468 Multiple breeding pairs for each population were housed together in 40-liter aquaria with
469 synthetic yarn spawning mops and fed ad libitum daily with frozen foods and commercial pellets.
470 Embryos were collected by handpicking and raised at 27°C in 5 ppt salinity water with the addition
471 of 10 mg/l gentamycin and 0.0001% methylene blue. Fertilization was confirmed after collection
472 and embryos were staged according to Lencer and McCune (2018). The day of collection was
473 noted as day "zero", and thus one day after collection was 1-day post-fertilization (dpf).

474

475 **HCR FISH staining**

476 Hybridization chain reaction (HCR) was used to visualize spatial expression of *galr2a* and *tpm3b*
477 at key development timepoints (Choi et al., 2018; Ibarra-García-Padilla et al., 2021). HCR
478 reagents, including probes, hairpins, and buffers, were purchased directly from Molecular
479 Instruments (Los Angeles, California, USA). Staining was performed according to a modified
480 protocol from Ibarra-García-Padilla et al., 2021, and Palominos and Whitlock, 2021.

481

482 *Fixation and storage:* 2 and 8 dpf larvae were fixed in 4% paraformaldehyde (Electron Microscopy
483 Science) 1X PBS (Invitrogen) overnight at 4°C. Samples were then serially dehydrated in

484 methanol/1X PBS (25%, 50%, 75%) and stored in 100% methanol at -20°C for at least 16 hours
485 before use. *Permeabilization:* Rehydration was performed serially in methanol/PBST (1X PBS
486 0.1% Tween20, Fisher Scientific) up to 100% PBST. Samples were then incubated for 10 minutes
487 in pre-chilled acetone at -20°C for permeabilization. 2 and 8 dpf samples were then incubated for
488 20 and 80 minutes in 10 µg/ml Proteinase K (Thermofisher), respectively. Prehybridization:
489 Samples were then pre-hybridized in the pre-warmed (at 37°C) hybridization buffer for 30 minutes
490 at 37°C. *Hybridization:* For *Galr2a* and *Tpm3,* 4 to 6 pmol and 2 to 3 pmol were used, respectively.
491 The probe mixture was pre-warmed for 30 minutes at 37°C before hybridization for 20 hours at
492 37°C. *Washing probe excess:* After hybridization, we performed four washes in pre-warmed wash
493 buffer (15 minutes each) at 37°C, followed by two final washes in 5X SSCT (20X SSC from
494 Thermofisher; SSCT is SSC with 0.1% Tween20) for 5 minutes each. *Amplification:*
495 Preamplification involved incubating samples in pre-equilibrated (20-25°C) amplification buffer
496 for 30 minutes. Next, amplification was performed using 4 µl of each snap-cooled hairpin in 250
497 µl of amplification buffer for 16 hours in the dark at room temperature. *Galr2a* expression was
498 confirmed independently using two amplifiers with different excitation/emission wavelengths: B1-
499 488 HCR amplifiers, and B1-594 HCR amplifiers. *Tpm3b* amplifiers used were B2-647 HCR
500 amplifiers. *Washing hairpin excess:* Excess hairpins were washed several times with 5X SSCT,
501 followed by a last wash with PBST. *Nuclei labeling:* After rinsing, samples were incubated for 30
502 minutes in DAPI/1X PBST (1 µm/ml, Sigma) and then washed in PBST 3 times for 5 minutes
503 each. *Clearing and mounting:* Samples were then serially cleared in glycerol solutions at room
504 temperature by sequentially removing and adding: 25% glycerol/75% PBST, 50% glycerol/50%
505 PBST, 75% glycerol/25% PBST. Samples were then mounted in a custom-made bridged
506 microscope slide (Fisher Scientific) in 75% glycerol/25% PBST.

507

508 *Imaging:* Samples were imaged using a Zeiss LSM880 (inverted) confocal microscope at the CNR
509 Biological Imaging Facility at the University of California, Berkeley. All HCR were volumetric z-
510 stack images of embryos or larvae positioned laterally or ventrally and taken every 3 µm. Images
511 were deconvoluted, analyzed, and edited in FIJI (Schindelin et al., 2012) and Imaris (Bitplane).

512

513 **Galr2 inhibition during jaw development**

514 According to the pupfish developmental series of Lencer and McCune (2018), the pharyngeal
515 arches of *C. variegatus* are visible as segmented pouches ventral to the developing head at Stage
516 25 (48-64 hours post-fertilization at 27 °C, or 2 – 2.5 dpf), while the presence of a stomodeum-
517 like oral cavity is evident by Stage 30 (100 – 130 hpf, or 4 – 5.5 dpf). We hypothesized that the
518 key stages for proper jaw development occur between Stages 24 and 25, and thus we dechorionated
519 Stage 24-25 embryos (or 2 to 2.5 dpf) pupfish by incubating them on 20 mg/ml Pronase (Roche)
520 in water for 2.5 hours. The remaining chorions were removed manually with forceps. After larvae
521 were dechorionated, we incubated them in 100 µM M35 (InnoPep Inc, San Diego, CA), a chimeric
522 peptide antagonist to all galanin receptors (Galr1 and Galr2 in teleost fishes; Butler et al. 2020)
523 and with a conserved 21 aminoacidic sequence to the core Galanin peptide sequence
524 (GWTLNSAGYLLGPPPGFSPFR-NH2), or M871 (Abcam, USA), a Galr2-specific antagonist
525 with the following aminoacidic sequence: WTLNSAGYLLGPEHPPPALALA-NH2), up to
526 hatching time (around 8 dpf, Stage 32-33).

527 *Cartilage staining:* a non-acid clearing and staining method was used based on Walker and
528 Kimmel, 2007, and Lencer and McCune, 2018. Fish larvae were cleared in 80% glycerol and
529 mounted in custom-made coverslips (Fisher Scientific). Meckel's length, inter-ocular distance, and

530 chondrocyte density were quantified using the segmented line tool and ROI manager in Fiji
531 (Schindelin et al., 2012). Imaging was done using a Zeiss Z1 AxioImager M2 microscope located
532 at the Biological Imagining Facility of the University of California, Berkeley.
533
534 **Sequencing of Galr2a regulatory alleles**
535 We used the DNeasy Blood and Tissue kit (Qiagen, Inc.) to extract DNA from the fins of wild-
536 caught adult fish and quantified it on a Qubit 3.0 fluorometer (Thermofisher Scientific, Inc.). All
537 specimens used in this study are kept in the Museum of Vertebrate Zoology at the University of
538 California, Berkeley. The primers used to amplify both *Galr2a* regulatory loci are listed in Table
539 S5. The sizes of the PCR products were confirmed by gel electrophoresis. PCR product clean-up
540 was done using ExoSap-IT (USB) and quantified on a Nanodrop ND-1000 (Thermo Scientific)
541 spectrophotometer. Sanger sequencing was performed at the UC Berkeley DNA Sequencing
542 Facility. Sequence alignment was performed using Geneious Prime (Dotmatics).
543
544 **Prediction of transcription factors binding sites in *Galr2a-15kb* and *Galr2a-12kb***
545 We used the Multiple Expectation maximizations for Motif Elicitation (MEME) server
546 (http://meme-suite.org/) and the motif database scanning algorithm TOMTOM (Bailey et al.,
547 2009) to retrieve TFBS motifs from a 20kb conserved generalist, molluscivore, and scale-eater
548 sequences upstream *galr2a* obtained from Richards et al., 2021. MEME suite finds, in the given
549 sequences, the most statistically significant motifs first. We numbered the motifs following their
550 statistical significance (Table S1).
551
552

553 **Statistics**

554 *Expression quantification of galr2a and tpm3b at 8 dpf:* We segmented and quantified "jaw"
555 *galr2a* expression in the maxilla, and the Meckel's and palatoquadrate cartilages and "brain"
556 *galr2a* expression in the central nervous system from HCR confocal images using 3D-Slicer
557 (Fedorov et al., 2012). *Tpm3b* expression was segmented and quantified in the intermandibular
558 muscles (IMA), the protractor hyoideus (PR-H), the adductor mandibular complex (AddM), and
559 the levator arcus palatini (LEVs). Muscles were named according to Diogo et al., 2008. Statistical
560 tests comparing the expression volume among species and tissues were performed in R (R Core
561 Team 2023). We tested for significant differences in means via ANOVA and contrasted groups
562 post-hoc using Tukey's HSD test.

563

564 *Expression quantification of garlr2a at 2 dpf:* From the HCR confocal images, a total volume of
565 45 µm containing the pharyngeal arches was projected using the maximum intensity tool in Fiji.
566 We selected two different tissues using ROI manager and quantified the relative fluorescence
567 normalized by the background fluorescence of the image. First, we selected the mandibular
568 mesenchyme plus the first and second pharyngeal arches (labeled in the figure "Pharyngeal
569 Arches"). Then, we de-selected the second pharyngeal arch, quantifying only the expression of
570 *galr2* in the mandibular mesenchyme and the first pharyngeal arch (labeled in the figure
571 "Mandibular arch"). We then tested for significant differences in means via ANOVA and post-hoc
572 analysis with Tukey's HSD in R.

573

574 *mRNA transcript analysis:* A table containing RPKM values of transcripts from Lencer and
575 McCune, 2017, datasets was obtained from the following Dryad repository,

576 doi:10.5061/dryad.mb3gb. Genes of interest were found with the Gene ID listed on NCBI. Gene
577 IDs are as follows: 106090243, 107092788, 107090827, 107096257, 107098818, and 107092130,
578 for *galr2a, galr2b, galr1a, galr1b, gal,* and *sox21b*, respectively. Statistical tests comparing
579 transcripts RPKM expression between species and developmental stages were performed in R,
580 testing for significant differences in means via ANOVA and post-hoc analysis with Tukey's HSD.
581
582 *Cartilage staining:* We compared chondrocyte density for significant differences in means using
583 pairwise post-hoc Tukey's HSD tests. We used a generalized linear model accounting for species
584 and treatment and their interaction. We chose to measure chondrocytes within the Meckel's
585 cartilage because it allows for a clear view of each cell at the symphysis.
586
587 **Author's contributions**
588 Conceptualization: MFP, CHM; Data Collection: MFP, VM, EJR; Statistical analyses: MFP;
589 Resources: CHM; Microscopy: MFP, VM; Original draft: MFP; Revising: MFP, EJR, CHM.
590
591 **Acknowledgments**
592 We thank Michelle St. John, David Tian, Mara Van Tassell, Chloe Clair, Dylan Chau, and Heidi
593 Buratti for valuable comments and discussion of the results. We thank Lydia Smith for her help
594 throughout the development of this project in the Evolutionary Genetics Lab at the University of
595 California, Berkeley. We are particularly thankful to Austin H. Patton, who extracted the *C.*
596 *brontotheroides* mRNA reads to create the HCR probes tested here, and for his insightful ideas
597 and comments on the early stages of this manuscript. We thank the Gerace Research Centre and
598 Troy Day for logistical support and the government of the Bahamas for permission to collect and

export samples. This research was funded by the National Science Foundation DEB CAREER grant #1749764, National Institutes of Health grant 5R01DE027052-02, the University of North Carolina at Chapel Hill, and the University of California, Berkeley to CHM.

References

Albertson, R. C., Cresko, W., Detrich, H. W. and Postlethwait, J. H. (2009). Evolutionary mutant models for human disease. *Trends in Genetics* **25**, 74–81.

Bonfante, B., Faux, P., Navarro, N., Mendoza-Revilla, J., Dubied, M., Montillot, C., Wentworth, E., Poloni, L., Varón-González, C., Jones, P., et al. (2021). A GWAS in Latin Americans identifies novel face shape loci, implicating VPS13B and a Denisovan introgressed region in facial variation. *Sci Adv* **7**,.

Boyle, E. A., Li, Y. I. and Pritchard, J. K. (2017). An Expanded View of Complex Traits: From Polygenic to Omnigenic. *Cell* **169**, 1177–1186.

Brawand, D., Wagner, C. E., Li, Y. I., Malinsky, M., Keller, I., Fan, S., Simakov, O., Ng, A. Y., Lim, Z. W., Bezault, E., et al. (2014). The genomic substrate for adaptive radiation in African cichlid fish. *Nature* **513**, 375–381.

Buffenstein, R. (2008). Negligible senescence in the longest living rodent, the naked mole-rat: Insights from a successfully aging species.

Carlborg, O. and Haley, C. S. (2004). Epistasis: too often neglected in complex trait studies? *Nature reviews. Genetics* **5**, 618–625.

619 **Chan, Y. F., Marks, M. E., Jones, F. C., Villarreal, G., Shapiro, M. D., Brady, S. D.,**
620 **Southwick, A. M., Absher, D. M., Grimwood, J., Schmutz, J., et al.** (2010). Adaptive
621 evolution of pelvic reduction in sticklebacks by recurrent deletion of a Pitx1 enhancer.
622 *Science (New York, N.Y.)* **327**, 302–305.

623 **Concannon, M. R. and Albertson, R. C.** (2015). The genetic and developmental basis of an
624 exaggerated craniofacial trait in East African cichlids. *J. Exp. Zool. B Mol. Dev. Evol.* **324**,
625 662–670.

626 **Conith, A. J., Lam, D. T. and Albertson, R. C.** (2019). Muscle-induced loading as an important
627 source of variation in craniofacial skeletal shape. *Genesis* **57**, e23263.

628 **Erickson, P. A., Glazer, A. M., Cleves, P. A., Smith, A. S. and Miller, C. T.** (2014). Two
629 developmentally temporal quantitative trait loci underlie convergent evolution of increased
630 branchial bone length in sticklebacks. *Proceedings of the Royal Society B: Biological*
631 *Sciences* **281**,.

632 **Erickson, P. A., Ellis, N. A. and Miller, C. T.** (2016). Microinjection for transgenesis and
633 genome editing in threespine sticklebacks. *J. Vis. Exp.* 10.3791/54055.

634 **Glazer, A. M., Killingbeck, E. E., Mitros, T., Rokhsar, D. S. and Miller, C. T.** (2015). Genome
635 assembly improvement and mapping convergently evolved skeletal traits in sticklebacks
636 with genotyping-by-sequencing. *Genes,Genomes,Genetics* **5**, 1463–1472.

637 **Glazier, A. M.** (2002). Finding genes that underlie complex traits. *Science (New York, N.Y.)* **298**,
638 2345–2349.

639 **Gross, J. B., Stahl, B. a., Powers, A. K. and Carlson, B. M.** (2016). Natural bone fragmentation
640 in the blind cave-dwelling fish, *Astyanax mexicanus*: Candidate gene identification through
641 integrative comparative genomics. *Evolution and Development* **18**, 7–18.

642 **Hall, D., Tegstrom, C. and Ingvarsson, P. K.** (2010). Using association mapping to dissect the
643 genetic basis of complex traits in plants. *Briefings in functional genomics* **9**, 157–165.

644 **Hawes, J. J., Narasimhaiah, R. and Picciotto, M. R.** (2006). Galanin and galanin-like peptide
645 modulate neurite outgrowth via protein kinase C-mediated activation of extracellular
646 signal-related kinase. *Eur. J. Neurosci.* **23**, 2937–2946.

647 **Helman, S. N., Badhey, A., Kadakia, S. and Myers, E.** (2014). Revisiting Crouzon syndrome:
648 reviewing the background and management of a multifaceted disease. *Oral and*
649 *Maxillofacial Surgery* **18**, 373–379.

650 **Hernandez, L. P., Adriaens, D., Martin, C. H., Wainwright, P. C., Masschaele, B. and**
651 **Dierick, M.** (2018). Building trophic specializations that result in substantial niche
652 partitioning within a young adaptive radiation. *J. Anat.* **232**, 173–185.

653 **Hirschhorn, J. N. and Daly, M. J.** (2005). Genome-wide association studies for common diseases
654 and complex traits. *Nature reviews* **6**, 95–108.

655 **Hochheiser, H., Aronow, B. J., Artinger, K., Beaty, T. H., Brinkley, J. F., Chai, Y., Clouthier,**
656 **D., Cunningham, M. L., Dixon, M., Donahue, L. R., et al.** (2011). The FaceBase
657 Consortium: A comprehensive program to facilitate craniofacial research. *Developmental*
658 *Biology* **355**, 175–182.

659 **Hofmann, C. M., O'Quin, K. E., Justin Marshall, N., Cronin, T. W., Seehausen, O. and**
660 **Carleton, K. L.** (2009). The eyes have it: Regulatory and structural changes both underlie
661 cichlid visual pigment diversity. *PLoS Biol.* **7**,.

662 **Humphries, J. M. and Miller, R. R.** (1981). A remarkable species flock of pupfishes, genus
663 *Cyprinodon*, from Yucatan, Mexico. *Copeia* **1981**, 52–64.

664 **J. Parsons, K., McWhinnie, K. and Armstrong, T.** (2021). An Evo-devo View of Post-genomic
665 African Cichlid Biology: Enhanced Models for Evolution and Biomedicine. In *The*
666 *Behavior, Ecology and Evolution of Cichlid Fishes* (ed. Abate, M. E.) and Noakes, D. L.
667 G.), pp. 779–802. Dordrecht: Springer Netherlands.

668 **Jones, F. C., Grabherr, M. G., Chan, Y. F., Russell, P., Mauceli, E., Johnson, J., Swofford,**
669 **R., Pirun, M., Zody, M. C., White, S., et al.** (2012). The genomic basis of adaptive
670 evolution in threespine sticklebacks. *Nature* **484**, 55–61.

671 **Kadakia, S., Helman, S. N., Badhey, A. K., Saman, M. and Ducic, Y.** (2014). Treacher Collins
672 Syndrome: The genetics of a craniofacial disease.

673 **Kocher, T. D.** (2004). Adaptive evolution and explosive speciation: The cichlid fish model. *Nat.*
674 *Rev. Genet.* **5**, 288–298.

675 **Kocher, T. D., Albertson, R. C., Carleton, K. L. and Streelman, J. T.** (2003). The genetic basis
676 of biodiversity, genomic studies of cichlid fishes. *Aquatic genomics: steps toward a great*
677 *future.* 34–44.

678 **Kolora, S. R. R., Owens, G. L., Vazquez, J. M., Stubbs, A., Chatla, K., Jainese, C., Seeto, K.,**
679 **McCrea, M., Sandel, M. W., Vianna, J. A., et al.** (2021). Origins and evolution of
680 extreme life span in Pacific Ocean rockfishes. *Science* **374**, 842–847.

681 **Lencer, E. S., Riccio, M. L. and McCune, A. R.** (2016). Changes in growth rates of oral jaw
682 elements produce evolutionary novelty in bahamian pupfish. *J. Morphol.* **277**, 935–947.

683 **Lencer, E. S., Warren, W. C., Harrison, R. and McCune, A. R.** (2017). The Cyprinodon
684 variegatus genome reveals gene expression changes underlying differences in skull
685 morphology among closely related species. *BMC Genomics* **18**, 424.

686 **Li, L., Wei, S., Huang, Q., Feng, D., Zhang, S. and Liu, Z.** (2013). A novel galanin receptor 1a
687 gene in zebrafish: tissue distribution, developmental expression roles in nutrition
688 regulation. *Comp. Biochem. Physiol. B Biochem. Mol. Biol.* **164**, 159–167.

689 **Liu, S., Lorenzen, E. D., Fumagalli, M., Li, B., Harris, K., Xiong, Z., Zhou, L., Korneliussen,**
690 **T. S., Somel, M., Babbitt, C., et al.** (2014). Population genomics reveal recent speciation
691 and rapid evolutionary adaptation in polar bears. *Cell* **157**, 785–794.

692 **Ma, A., Bai, J., He, M. and Wong, A. O. L.** (2018). Spexin as a neuroendocrine signal with
693 emerging functions. *Gen. Comp. Endocrinol.* **265**, 90–96.

694 **Mack, K. L. and Nachman, M. W.** (2017). Gene Regulation and Speciation. *Trends Genet.* **33**,
695 68–80.

Man, P.-S. and Lawrence, C. B. (2008). The effects of galanin-like peptide on energy balance, body temperature and brain activity in the mouse and rat are independent of the GALR2/3 receptor. *J. Neuroendocrinol.* **20**, 128–137.

Manolio, T. A., Collins, F. S., Cox, N. J., Goldstein, D. B., Hindorff, L. A., Hunter, D. J., McCarthy, M. I., Ramos, E. M., Cardon, L. R., Chakravarti, A., et al. (2009). Finding the missing heritability of complex diseases. *Nature* **461**, 747–753.

Martin, C. H. (2012). Weak disruptive selection and incomplete phenotypic divergence in two classic examples of sympatric speciation: Cameroon crater lake cichlids. *Am. Nat.* **180**, E90–E109.

Martin, C. H. (2013). Strong assortative mating by diet, color, size, and morphology but limited progress toward sympatric speciation in a classic example: Cameroon crater lake cichlids. *Evolution* **67**, 2114–2123.

Martin, C. H. (2016). The cryptic origins of evolutionary novelty: 1000-fold faster trophic diversification rates without increased ecological opportunity or hybrid swarm. *Evolution*.

Martin, C. H. and Genner, M. J. (2009). High niche overlap between two successfully coexisting pairs of Lake Malawi cichlid fishes. *Canadian Journal of Fisheries and Aquatic Sciences* **66**, 579–588.

Martin, C. H. and Gould, K. J. (2020). Surprising spatiotemporal stability of a multi-peak fitness landscape revealed by independent field experiments measuring hybrid fitness. *Evol Lett* **4**, 530–544.

716 **Martin, C. H. and Wainwright, P. C.** (2011). Trophic novelty is linked to exceptional rates of
717 morphological diversification in two adaptive radiations of *Cyprinodon* pupfishes.
718 *Evolution* **65**, 2197–2212.

719 **Martin, C. H. and Wainwright, P. C.** (2013a). A remarkable species flock of *Cyprinodon*
720 pupfishes endemic to San Salvador Island, Bahamas. *Bulletin of the Peabody Museum of*
721 *Natural History* **54**, 231–240.

722 **Martin, C. H. and Wainwright, P. C.** (2013b). Multiple fitness peaks on the adaptive landscape
723 drive adaptive radiation in the wild. *Science (New York, N.Y.)* **339**, 208–211.

724 **Martin, C. H., Cutler, J. S., Friel, J. P., Dening, T., Coop, G. and Wainwright, P. C.** (2015).
725 Complex histories of repeated colonization and hybridization cast doubt on the clearest
726 examples of sympatric speciation in the wild. *Evolution* **69**, 1406–1422.

727 **Martin, C. H., Erickson, P. A. and Miller, C. T.** (2017). The genetic architecture of novel trophic
728 specialists: higher effect sizes are associated with exceptional oral jaw diversification in a
729 pupfish adaptive radiation. *Molecular Ecology* **26**, 624–638.

730 **Martin, C. H., McGirr, J. A., Richards, E. J. and St John, M. E.** (2019). How to Investigate
731 the Origins of Novelty: Insights Gained from Genetic, Behavioral, and Fitness
732 Perspectives. *Integr Org Biol* **1**, obz018.

733 **Matsumoto, Y., Watanabe, T., Adachi, Y., Itoh, T., Ohtaki, T., Onda, H., Kurokawa, T.,**
734 **Nishimura, O. and Fujino, M.** (2002). Galanin-like peptide stimulates food intake in the
735 rat. *Neurosci. Lett.* **322**, 67–69.

736 **McGirr, J. A. and Martin, C. H.** (2016). Novel candidate genes underlying extreme trophic
737 specialization in Caribbean pupfishes. *Molecular Biology and Evolution* **34**, 873–888.

738 **McGirr, J. A. and Martin, C. H.** (2021). Few Fixed Variants between Trophic Specialist Pupfish
739 Species Reveal Candidate Cis-Regulatory Alleles Underlying Rapid Craniofacial
740 Divergence. *Mol. Biol. Evol.* **38**, 405–423.

741 **Meng, L., Bian, Z., Torensma, R. and Von den Hoff, J. W.** (2009). Biological mechanisms in
742 palatogenesis and cleft palate. *Journal of Dental Research* **88**, 22–23.

743 **Miller, C. T., Beleza, S., Pollen, A. A., Schluter, D., Kittles, R. A., Shriver, M. D. and**
744 **Kingsley, D. M.** (2007). cis-Regulatory changes in Kit ligand expression and parallel
745 evolution of pigmentation in sticklebacks and humans. *Cell* **131**, 1179–1189.

746 **Monteiro, A. and Podlaha, O.** (2009). Wings, horns, and butterfly eyespots: how do complex
747 traits evolve? *PLoS biology* **7**, e37.

748 **Naqvi, S., Hoskens, H., Wilke, F., Weinberg, S. M., Shaffer, J. R., Walsh, S., Shriver, M. D.,**
749 **Wysocka, J. and Claes, P.** (2022). Decoding the Human Face: Progress and Challenges
750 in Understanding the Genetics of Craniofacial Morphology. *Annu. Rev. Genomics Hum.*
751 *Genet.*

752 **Navon, D., Male, I., Tetrault, E. R., Aaronson, B., Karlstrom, R. O. and Albertson, R. C.**
753 (2020). Hedgehog signaling is necessary and sufficient to mediate craniofacial plasticity in
754 teleosts. *Proc. Natl. Acad. Sci. U. S. A.* **117**, 19321–19327.

755 **Palmer, K., Fairfield, H., Borgeia, S., Curtain, M., Hassan, M. G., Dionne, L., Yong Karst,**
756 **S., Coombs, H., Bronson, R. T., Reinholdt, L. G., et al.** (2016). Discovery and
757 characterization of spontaneous mouse models of craniofacial dysmorphology.
758 *Developmental Biology* **415**, 216–227.

759 **Pavlidis, P., ??ivkovi??, D., Stamatakis, A. and Alachiotis, N.** (2013). SweeD: Likelihood-
760 based detection of selective sweeps in thousands of genomes. *Mol. Biol. Evol.* **30**, 2224–
761 2234.

762 **Platzer, M. and Englert, C.** (2016). *Nothobranchius furzeri*: A model for aging research and
763 more. *Trends in Genetics* **32**, 543–552.

764 **Powder, K. E. and Albertson, R. C.** (2016). Cichlid fishes as a model to understand normal and
765 clinical craniofacial variation. *Developmental Biology* **415**, 338–346.

766 **Price, A. L., Spencer, C. C. A. and Donnelly, P.** (2015). Progress and promise in understanding
767 the genetic basis of common diseases. *Proceedings of the Royal Society B: Biological*
768 *Sciences* **282**, 20151684.

769 **Protas, M., Conrad, M., Gross, J. B., Tabin, C. and Borowsky, R.** (2007). Regressive evolution
770 in the Mexican cave tetra, Astyanax mexicanus. *Current biology : CB* **17**, 452–454.

771 **Reardon, W., Winter, R. M., Rutland, P., Pulleyn, L. J., Jones, B. M. and Malcolm, S.** (1994).
772 Mutations in the fibroblast growth factor receptor 2 gene cause Crouzon syndrome. *Nature*
773 *Genetics* **8**, 98–103.

774 **Richards, E. J. and Martin, C. H.** (2017). Adaptive introgression from distant Caribbean islands
775 contributed to the diversification of a microendemic adaptive radiation of trophic specialist
776 pupfishes. *PLoS Genet.* **13**, 1–35.

777 **Richards, E. J. and Martin, C. H.** (2022). We get by with a little help from our friends: shared
778 adaptive variation provides a bridge to novel ecological specialists during adaptive
779 radiation. *Proc. Biol. Sci.* **289**, 20220613.

780 **Richards, E. J., McGirr, J. A., Wang, J. R., St John, M. E., Poelstra, J. W., Solano, M. J.,**
781 **O'Connell, D. C., Turner, B. J. and Martin, C. H.** (2021). A vertebrate adaptive
782 radiation is assembled from an ancient and disjunct spatiotemporal landscape. *Proc. Natl.*
783 *Acad. Sci. U. S. A.* **118**,.

784 **Roberts, R. B., Ser, J. R. and Kocher, T. D.** (2009). Sexual conflict resolved by invasion of a
785 novel sex determiner in Lake Malawi cichlid fishes. *Science (New York, N.Y.)* **326**, 998–
786 1001.

787 **Roberts, R. B., Hu, Y., Albertson, R. C. and Kocher, T. D.** (2011). Craniofacial divergence and
788 ongoing adaptation via the hedgehog pathway. *Proceedings of the National Academy of*
789 *Sciences of the United States of America* **108**, 13194–13199.

790 **Rohner, N.** (2018). Cavefish as an evolutionary mutant model system for human disease. *Dev.*
791 *Biol.* **441**, 355–357.

792 **Signor, S. A. and Nuzhdin, S. V.** (2018). The Evolution of Gene Expression in cis and trans.
793 *Trends Genet.* **34**, 532–544.

794 **Sollenberg, U. E., Lundström, L., Bartfai, T. and Langel, Ü.** (2006). M871—A Novel Peptide
795 Antagonist Selectively Recognizing the Galanin Receptor Type 2. *Int. J. Pept. Res. Ther.*
796 **12**, 115–119.

797 **Sollenberg, U. E., Runesson, J., Sillard, R. and Langel, Ü.** (2010). Binding of Chimeric Peptides
798 M617 and M871 to Galanin Receptor Type 3 Reveals Characteristics of Galanin Receptor–
799 Ligand Interaction. *Int. J. Pept. Res. Ther.* **16**, 17–22.

800 **St John, M. E., Holzman, R. and Martin, C. H.** (2020a). Rapid adaptive evolution of scale-
801 eating kinematics to a novel ecological niche. *J. Exp. Biol.* **223**,.

802 **St John, M. E., Dixon, K. E. and Martin, C. H.** (2020b). Oral shelling within an adaptive
803 radiation of pupfishes: Testing the adaptive function of a novel nasal protrusion and
804 behavioural preference. *J. Fish Biol.* **97**, 163–171.

805 **St. John, M. E., Dunker, J. C., Richards, E. J., Romero, S. and Martin, C. H.** (2021). Parallel
806 genetic changes underlie integrated craniofacial traits in an adaptive radiation of trophic
807 specialist pupfishes. *bioRxiv* 2021.07.01.450661.

808 **Sutter, N. B., Bustamante, C. D., Chase, K., Gray, M. M., Zhao, K., Zhu, L.,**
809 **Padhukasahasram, B., Karlins, E., Davis, S., Jones, P. G., et al.** (2007). A single IGF1
810 allele is a major determinant of small size in dogs. *Science (New York, N.Y.)* **316**, 112–115.

811 **Venn-watson, S., Carlin, K. and Ridgway, S.** (2011). General and Comparative Endocrinology
812 Dolphins as animal models for type 2 diabetes : Sustained , post-prandial hyperglycemia
813 and hyperinsulinemia. *General and Comparative Endocrinology* **170**, 193–199.

814 **Weinberg, S. M., Cornell, R. and Leslie, E. J.** (2018). Craniofacial genetics: Where have we
815 been and where are we going? *PLoS Genet.* **14**, e1007438.

816 **Wilkie, A. O., Slaney, S. F., Oldridge, M., Poole, M. D., Ashworth, G. J., Hockley, A. D.,**
817 **Hayward, R. D., David, D. J., Pulleyn, L. J. and Rutland, P.** (1995). Apert syndrome
818 results from localized mutations of FGFR2 and is allelic with Crouzon syndrome. *Nature*
819 *genetics* **9**, 165–172.